ELSEVIER

International Journal of Mass Spectrometry 192 (1999) 393–405

International Journal of Mass Spectrometry

Scattering of multiply charged ions from surfaces

N. Hatke[a], A. Robin[a], M. Grether[b], A. Närmann[c], W. Heiland[a]*

[a]*Universität Osnabrück, D-49069 Osnabrück, Germany*
[b]*Hahn-Meitner-Institut, Berlin, D-14109 Berlin, Germany*
[c]*Technische Universität Clausthal, D-38678 Clausthal-Zellerfeld, Germany and KVI Atoomfysica, NL-9747 AA Groningen, The Netherlands*

Received 23 November 1998; accepted 11 March 1999

Abstract

We have measured surface channeling and resonant coherent excitation of N^{6+} ions scattered off a Pt(110)(1 × 2) surface at energies of 23.0 MeV and 21.8 MeV. In order to achieve surface channeling at those energies small grazing angles of incidence below 0.10° must be achieved. When scattered at 21.8 MeV along the [110] surface semichannels resonant coherent excitation (RCE) is observed. The effect is studied as a function of the azimuthal angle and the angle of incidence. The experimental findings agree with earlier bulk channeling experiments. In comparison with theoretical predictions satisfactory agreement is found. (Int J Mass Spectrom 192 (1999) 393–405) © 1999 Elsevier Science B.V.

Keywords: Multiply charged ions; Resonant coherent excitation; Surface channeling

1. Introduction

The study of the interaction of multiply charged ions (MCI) with surfaces is stimulated, apart from scientific curiosity regarding the presence of MCI in TOKAMAK plasmas, for the effect of enhanced, potential energy induced sputtering of insulators and the formation of "hollow" atoms by the neutralisation effects at solid surfaces [1]. The MCI in plasmas are important for plasma diagnostics but they also play a role in the plasma-wall interaction. Because of the large potential energy of MCI, e.g. for slow ions the potential energy can be larger than the kinetic energy, it has been envisaged that a gentle sputtering process may be possible. In this sputtering process the damage caused by the energy deposition of a fast ion may be avoided. The originally proposed Coulomb explosion mechanism for the sputtering has not been verified. The enhanced sputtering found in the case of, e.g. LiF and SiO_2, is due to the well known mechanism involving self-trapped excitons [1]. The scattering and penetration of MCI off or into solids leads to the formation of electron emission processes that give insight into the charge capture from the solid into the MCI. The capture can happen outside the solid and can be understood in terms of the "over-barrier" model [2]. When the MCI approach a surface the surface barrier is lowered and electrons flow or hop back and forth between filled (empty) states of the solid and empty (filled) shell states of the MCI. Eventually the MCI are completely neutralised, but contain inner shell vacancies. It is this state of the

* Corresponding author. E-mail: wheiland@physik.uni-osnabrueck.de

PII S1387-3806(99)00090-1

MCI for which the phrase "hollow atom" was coined. Upon entering the solid some of the outer electrons may get lost and inside the solid new filling mechanisms take over [1–4]. If MCI are backscattered, which occurs at low "perpendicular" energies, the survival of inner shell holes of the scattered ions is observed [1,5]. The term "perpendicular" energy refers to the product of the kinetic energy of the incident MCI multiplied by $\sin^2\psi$ where ψ is the angle of incidence measured against the surface. This definition is related to the channeling effect for which a critical angle is defined relative to a crystallographic plane or axis, respectively. For angles smaller than this critical angle the ions are forced onto a guided trajectory due to a sequence of correlated small angle collisions [6]. For channeled particles the energy loss due to collisions with individual atoms (nuclear loss) is small compared to the energy loss due to excitation of the electronic systems of the target and the projectile (inelastic or electronic loss). Experiments with surface channeled ions therefore afford the study of electronic processes in good approximation independent of nuclear scattering processes [7].

Here we report the results of an experiment with fast MCI, i.e. $^{15}N^{6+}$, scattering off a Pt(110) surface and grazing angles of incidence. The aim of the experiment is the study of the resonant coherent excitation (RCE) effect. RCE was predicted to occur because of the simple concept that a string of atoms with lattice constant d provides a periodic potential for a particle scattering along that chain [8]. The periodic potential induced on the particle can cause an internal electronic excitation if the excitation energy $E = khv/d$, where $k = 1,2,3, \ldots$ is a constant describing the harmonic of the excitation, h is Planck's constant, and v is the particle velocity. The original proposal for the experimental verification of RCE was not successful, i.e. the enhanced light emission predicted for the scattering of He along a single crystal was not found [9,10]. This failure is due to the fact that the orbits of higher n states of He are too large to survive long enough for RCE near a surface. Consequently, the first successful experiments made use of highly charged, i.e. hydrogen-like, heavier ions, in which the orbits of the 1s states are small enough to get coherently excited into 2s, 2p states [11–13]. The 2s, 2p states in turn are so large that the ion eventually loses the excited electron. The signature of RCE in these experiments are hence minima in the ion ratio, e.g. N^{6+}/N^{7+}, as a function of the primary energy (velocity v) for channeling along a given axis of a single crystal. In the most recent experiment [13] of the Oak Ridge group the second possibility for observing RCE was used, i.e. the beam energy was kept constant and the azimuthal angle in a planar channeling situation was varied. More recently RCE experiments were extended to surfaces. B^{3+} ions where scattered off SnTe surfaces along a specific direction of the surface [14–16]. The B^{4+}/B^{5+} yield shows the expected RCE when the energy is varied around 5.5 MeV. Angles of incidence as low as $\psi = 0.11°$ to $\psi = 0.35°$ are used, corresponding to perpendicular energies of 22–199 eV, respectively. Obviously, only at the lowest angles of incidence are the conditions for surface channeling met. The reasons for the more stringent conditions for surface channeling are due to the difference between channeling and hyperchanneling. Channeling allows particles to wander between different axial or planar channels within a solid as long as the conditions of correlated collisions, described by continuous potentials and conservation of perpendicular momentum, are met. In the case of hyperchanneling the projectiles are bound to individual axial channels or individual planar channels. For surface channeling this usually means penetration into the bulk, where, of course, different physical properties are probed, e.g. different electron densities. Perpendicular energies below ~20 eV are necessary for hyperchanneling [7,11,17]. In our own experiments we repeated the bulk experiment of the Oak Ridge group very closely using 21.8 MeV N^{6+} as projectiles and Pt(110), instead of Au, as the target [18,19]. We used Pt(110) because of its better defined surface structure compared to Au(110). In this article we will present the RCE data of our experiment in full detail. RCE was observed for $\psi = 0.03°$, corresponding to a perpendicular energy of 5.97 eV. A low energy RCE experiment using H as the projectile was reported with LiF as the target [20]. Here the change of charge is not used as the signature of the RCE, but the

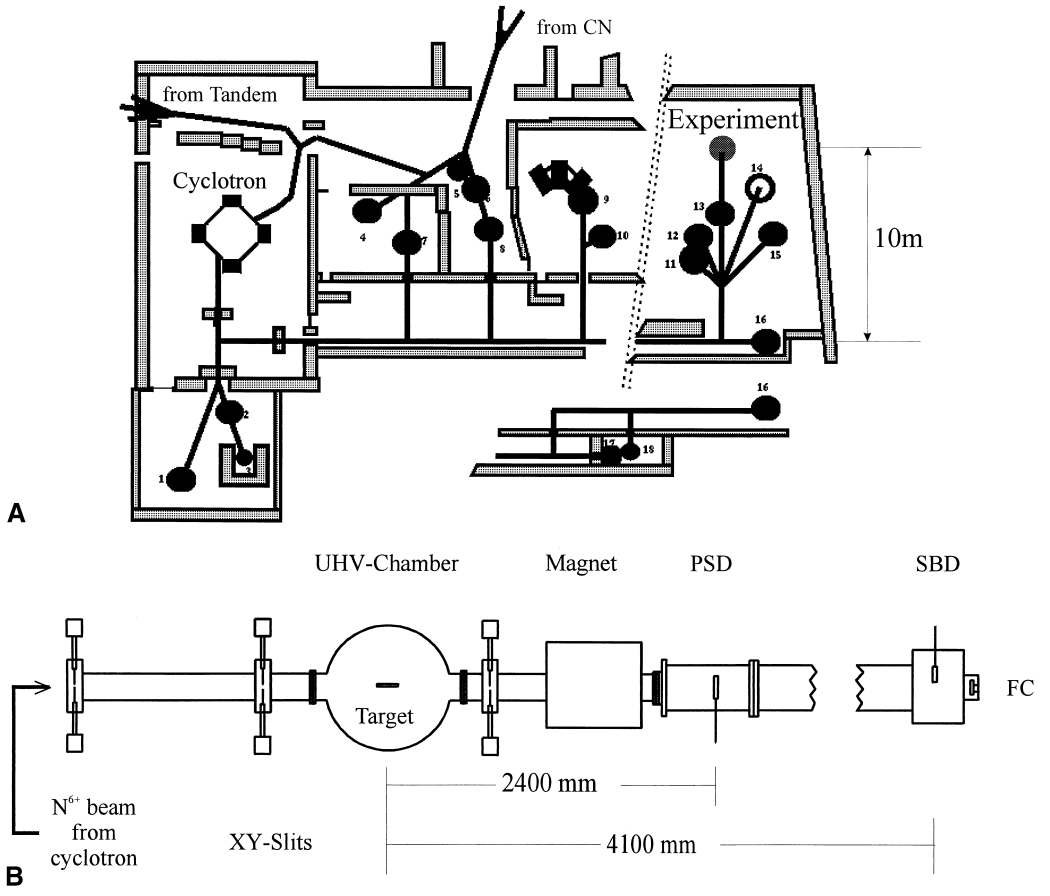

Fig. 1. (a) Ion beam facilities of the ISL (Ionen-Strahl-Labor: www.hmi.de) of the Hahn-Meitner Institut, Berlin. Position 1, e.g. is the eye-tumor treatment facility. Our experiment is located in the upper right hand corner. (b) Scheme of the surface channeling experiment. PSD = position sensitive detector; SBD = surface barrier detector; FC = Faraday cup.

emission of Lyman-α radiation due to excitation of H 1*s* to H 2*p*. At energies around 5.5 keV and angles of incidence from 0.3–2.5° the perpendicular energies vary from 0.15 to 10 eV, and are hence well in the range of hyperchanneling. In this experiment both the projectile energy and the azimuthal angle are varied in order to look into the "sidebands" of RCE [13,20].

2. Experiment

The experiments described here were done at the ISL (Ionen–Strahl–Labor: www.hmi.de) of the HMI (Hahn-Meitner Institut) at Berlin. The ISL provides MeV beams of highly charged ions with excellent energy definition because of the use of a cyclotron for the energy stabilisation. The experimental setup is shown in Fig. 1(a), giving an overview of the ISL beam facility. The primary ions are produced in an electron cyclotron resonance (ECR) ion source, accelerated in the 6 MV van de Graff and then fed into the cyclotron and accelerated to 24 MeV. For the definition of the final charge state and energy, carbon foils of appropriate thickness (approximately 400 μg/cm^2) are used. The $^{15}N^{6+}$ ions are charge selected by magnets after the cyclotron. The energy of the ions is controlled by means of nuclear magnetic resonance (NMR), thus affording a precise control of the deflecting magnet. The final beam definition system, target

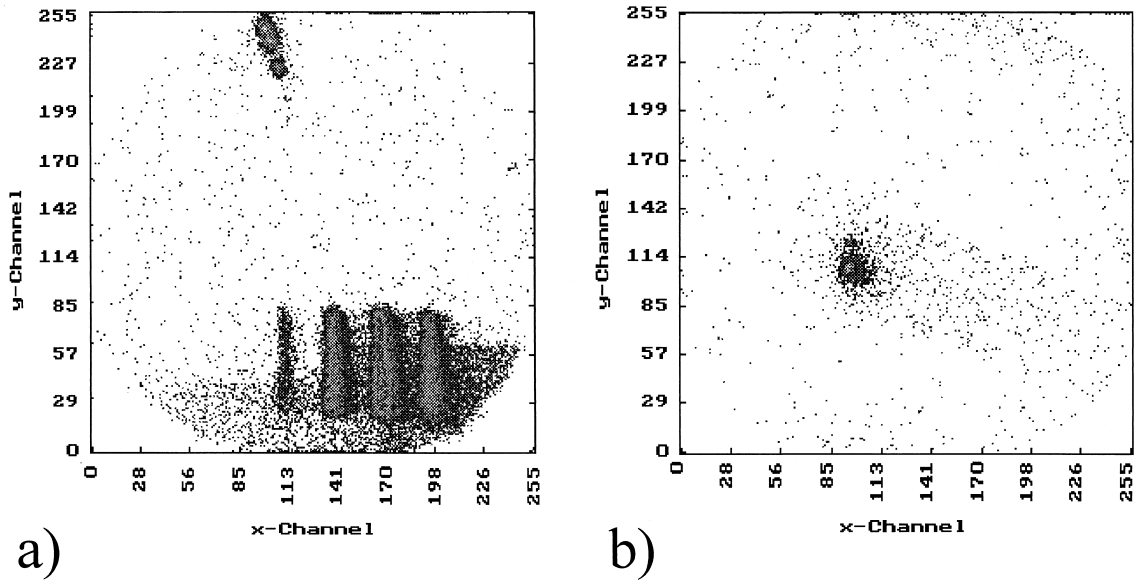

Fig. 2. Images of a "bad" (a) and a "good" (b) primary $^{15}N^{6+}$ 21.8. MeV magnetically analyzed beam. In case (a) the beam projects the shape of the *XY* slits onto the PSD. The different spots are due to different charge states from charge pickup somewhere in the beam line. (a) also shows the resolving power of the magnet. The feature on top of (a) is a defect (crack) of the front channel plate of the PSD. In (b) this channel plate was replaced.

chamber, and the arrangement of the different detectors used is shown schematically in Fig. 1(b). Beam preparation is composed primarily of two Faraday cups and two diaphragms with four movable slits. The slits (4 jaw slits) of the diaphragms also afford a readout of the current by which they are hit. This system serves first of all for putting the beam dead center on the axis of the experiment, i.e. of the target chamber, and cutting the cross section down to 0.2×0.2 mm^2. At this state the slits and the Faraday cup read hardly any current, so the fine tuning of the beam is done using a position sensitive detector (PSD) located behind the analysing magnet. The PSD is mounted on a linear motion feedthrough and can be moved out of the beam to use the downstream Faraday cup or the surface barrier detector (SBD). The magnet affords the charge state analysis of the beam that is simply displayed by the PSD (Fig. 2). Naturally, the beam size and shape is also visualised by the PSD. The PSD is a set of channel plates followed by a position resistive anode (Surface Science Lab, Mountain View, CA). The software used to process the data is described in detail elsewhere [21]. The beam energy distribution is analysed by a SBD that is mounted on a linear motion feedthrough at the very end of the beam line. The SBD is a Li drifted Si detector (Canberra PD 100-12-300AB). The output of the SBD is handled using standard particle counting electronics [22]. The SBD is calibrated and its energy resolution measured using a ^{241}Am α source. The linearity of the energy scale is checked by the ^{241}Am 5.486 MeV line and the 21.8 MeV and 23 MeV N^{6+} primary beams. The energy resolution is 22 keV full width at half maximum at 5.486 MeV. The width of the primary 21.8 MeV N^{6+} beam is 30 keV.

The target chamber is shown schematically in Fig. 3. It is an ultra high vacuum (UHV) stainless steel chamber with μ-metal screening. The base pressure in the chamber is in the 10^{-10} mbar range with the beam running. The upper part of the system is used for target preparation and analysis. The target is sputtered with 1 keV Ar ions and annealed at 600 °C until a brilliant, small spot low energy electron diffraction (LEED) (1×2) pattern is observed. The LEED

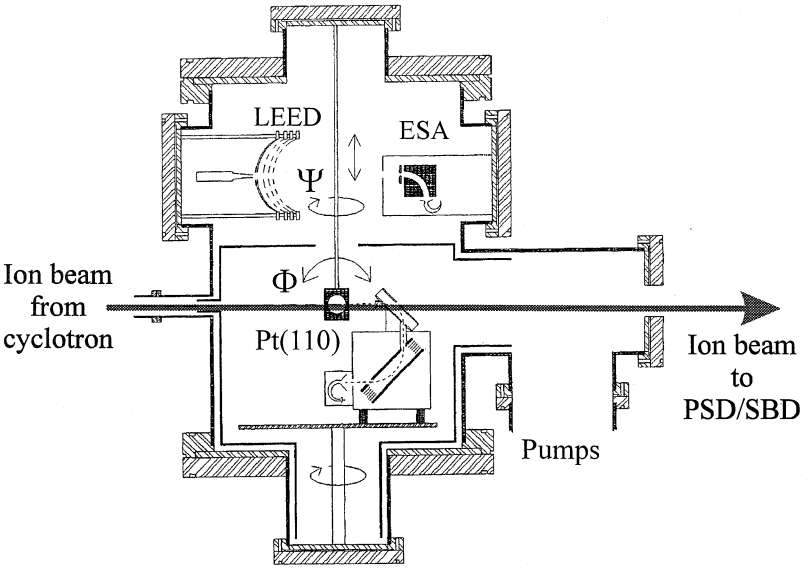

Fig. 3. Scheme of the target chamber (UHV). ψ is the (grazing) angle of incidence, ϕ is the azimuthal angle.

pattern also serves for the calibration of the azimuthal angle. From experiments on the same crystal surface using LEED and scanning tunneling microscopy (STM) [23] we know that such a LEED pattern is reproducibly correlated with a well defined surface structure. The "fish scale" surface terraces extend over several 100 Ångstrom with an average length in the $\langle 1\bar{1}0\rangle$ surface direction of 600 Å. The $\langle 110\rangle$ chains of the surface are the closed packed rows of the fcc structure with an atomic distance of 2.77 Å. The (1×2) structure of Pt(110) is a "missing row" structure, i.e. every second $\langle 1\bar{1}0\rangle$ row is missing. This structural detail has to be considered when analysing the particle trajectories along the surface. The chemical state of the surface is measured using an electrostatic analyser and low energy ions, i.e. by applying low energy ion scattering spectrometry (LEIS) [7]. In the lower part of the chamber the beam scattering and electron spectroscopy is performed. The electron spectroscopy experiments have been reported elsewhere [1]. The angle of incidence ψ and the azimuthal orientation ϕ are controlled by the manipulator (Fig. 3) using stepping motors.

For the surface channeling experiments the angle of incidence is the most important parameter. In order to reach perpendicular energies around 20 eV, angles below 0.06° are necessary at beam energies of 20 MeV. There is no goniometer or target manipulator with such a capability. In this situation the PSD is the only available means to control the scattering angle. From the PSD data the primary beam and the scattered beam positions are read, providing the scattering angle and hence the angle of incidence. Fig. 4(a) shows a 23 MeV $^{15}N^{6+}$ primary beam spatial distribution and Fig. 4(b) shows the primary beam and the scattered beam [19]. Note that the primary beam in Fig. 4(b) is cut down at the left hand side because of the presence of the target. It illuminates the experimental procedure, i.e. the target is first moved out of the beam [Fig. 4(a)] and aligned at best parallel to the beam. In the next step the target is moved parallel to the beam until the beam intensity (total counts of the PSD) is appreciably reduced to, e.g. $\sim$0.5 of the incident current. A suitable small angle of incidence is then adjusted by using the stepping motor control of the manipulator.

The analysing sector field magnet affords the charge state analysis, and, naturally, a momentum analysis. At fields of 10–60 mT, controlled by a Hall probe, the different charge states of N are separated

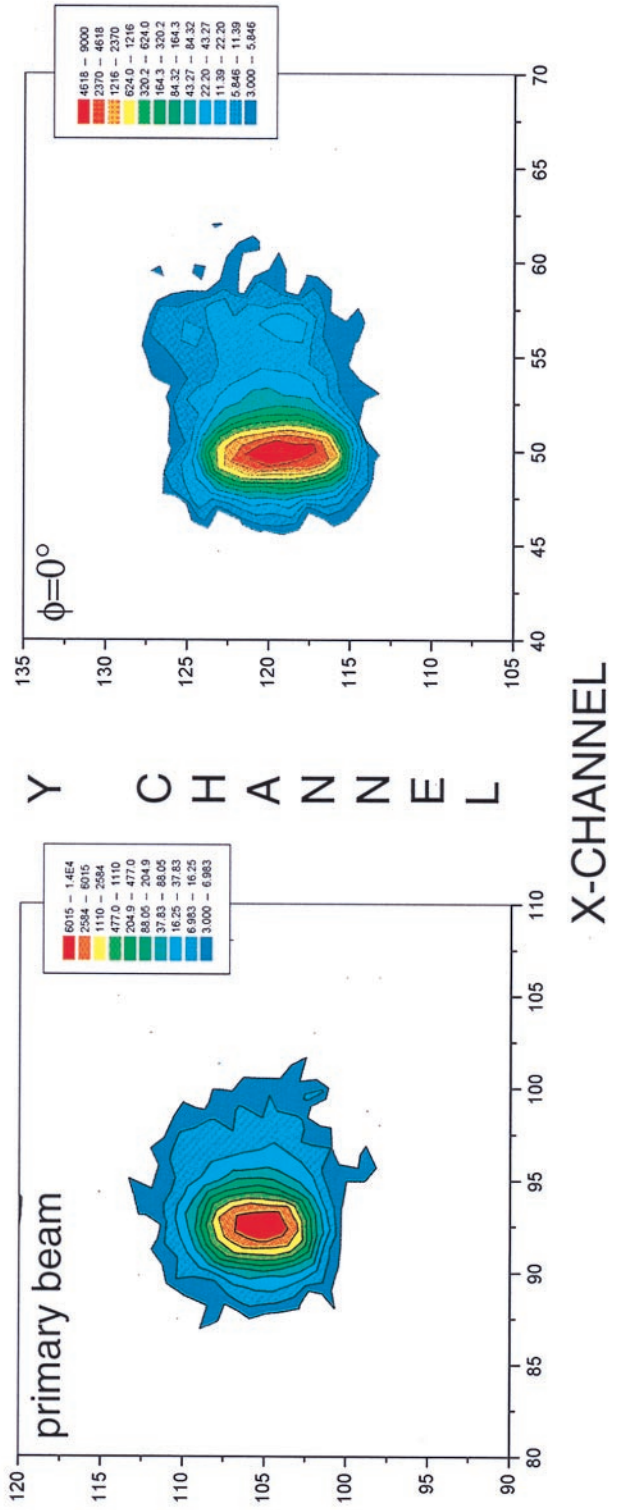

Fig. 4. (a) Intensity distribution of a 23 MeV $^{15}N^{6+}$ beam measured by the PSD. The color code is logarithmic in steps of factor 2. (b) Intensity distribution of a 23 MeV $^{15}N^{6+}$ scattered from Pt(110) at an angle of incidence of $\Psi = 0.03°$ (right spot) and half of the primary beam (left spot).

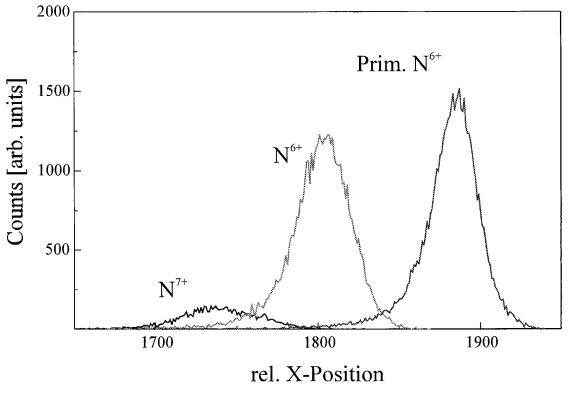

Fig. 5. Energy distributions of a primary $^{15}N^{6+}$, a scattered $^{15}N^{6+}$, and a scattered $^{15}N^{7+}$ beam measured with the surface barrier detector (SBD) (from right to left). The SBD is at a fixed position. Each energy distribution is measured at a different setting of the analyzing magnet, so the energy scales of the spectra are shifted, i.e. the *x* scale has no common energy scale, but the relative scales are identical.

by millimeters on the PSD (Fig. 2) and can be well resolved on the SBD (Fig. 5). The combination of magnet and SBD provides momentum, charge state, and energy analysis of the scattered particles, which is a unique feature, in comparison with other experiments. For the SBD experiment the target is moved further into the beam without changing the incident angle in order to reduce the primary beam intensity. This reduction is necessary to prolong the lifetime of the SBD and to minimize the overflow of the primary beam intensity into the scattered beam spectra.

3. Theoretical aspects of channeling and RCE

Channeling has been theoretically described by J. Lindhard [6] in connection with the shadow cone effect. Behind an atom hit by a parallel beam of ions a shadow cone is formed, such that atoms within this shadow cone cannot be hit at small impact parameters. If we have a row of atoms, each atom forms its shadow cone. Consequently, if the angle of incidence is smaller than a critical angle, the projectiles interact with this row of atoms at large impact parameters only. Under these conditions a row of atoms (or a plane of atoms) can be described by a cylindrical (or planar) continuous potential. Depending on the energy range the potentials are either Coulomb potentials or screened Coulomb potentials at high and low energies, respectively. This has two consequences, i.e. the perpendicular momentum of the ions is conserved and the motion of the ions is guided by the rows or planes. For given atomic numbers of the projectile, Z_1, and the target atoms, Z_2, the primary energy E, and a string of atoms with Miller indices $[hkl]$, the characteristic angle for axial channeling is:

$$\psi_1 = \sqrt{2Z_1Z_2e^2/Ed_{[hkl]}} \tag{1}$$

where e is the electron charge; here, $e = 14.4$ eV Å is useful, if E is given in eV and d in Å. Numerical calculations and experiments show that the actual critical angles $\psi_{\text{crit}} = 0.5\psi_1$. At low energies the screening length a_{12} of the potential used has to be taken into account and the critical angle can be estimated from:

$$\psi_2 = \sqrt{C'a_{12}\psi_{\text{crit}}/d_{[hkl]}} \tag{2}$$

where C' is a constant depending on the potential parameters and the thermal vibrational amplitudes. The numerical value of C' is of the order of 1 [24]. Note that at low energies the dependence on the lattice parameter is $1/d$ and on E it is $E^{-1/4}$ [25]. Low energies are defined by

$$E < 2e^2Z_1Z_2d_{[hkl]}/a_{12}^2 \tag{3}$$

The critical angles for planar channeling, which we will not use here, can be derived accordingly. A useful approximation for a "back of the envelope" estimate of critical angles is the "breakthrough" angle ψ_b, defined by the equality of the repulsive potential $V(r/a_{12})$ and the "perpendicular" component of the energy $E_\perp$ [25]:

$$V(r/a_{12}) = E\sin^2\psi_b \approx E\psi_b^2 \tag{4}$$

At energies above this $E_\perp$ projectiles penetrate into the bulk and hence surface channeling is lost. Numerical estimates show that ψ_b is in general smaller than the critical angles ψ_{crit}, which is to be expected, because ψ_b can be understood as a definition for the

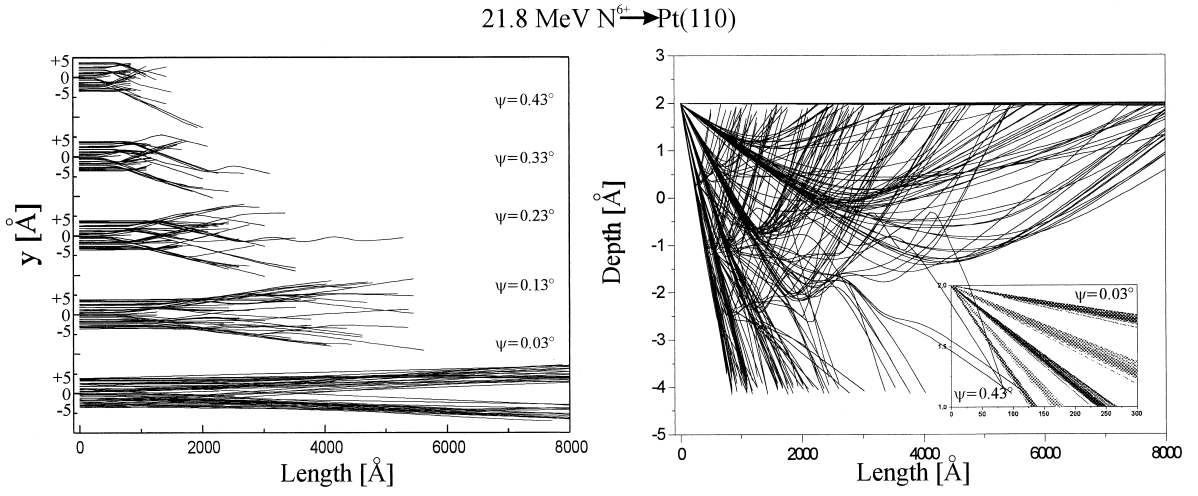

Fig. 6. Calculated trajectories of 21.8 MeV N^{6+} ions scattering off a Pt(110)(1 × 2) surface for different angles of incidence Ψ, top view and side view. Note the different *x* and *y* scales. The azimuthal orientation is $\phi = 0°$, i.e. parallel to the $\langle 1\bar{1}0\rangle$ surface channels of Pt(110)(1 × 2) the inset facilitates distinguishing the different angles of incidence in the side view presentation.

critical angle of hyperchanneling. The estimates show that $E_\perp$ is of the order of 10–20 eV [25]. Fig. 6 shows trajectories calculated for 21.8 MeV N ions scattering from a Pt(110)(1 × 2) surface. The results are based on solving Newton's equations for ions interacting with a model surface of 5 × 5 Pt atoms whose potentials overlap. The potential used is a Ziegler–Biersack–Littmark (ZBL) potential [26]. It is clearly shown that breakthrough starts at approximately $\psi > 0.10°$, the evidence being trajectories that go beyond −2.8 Å, the position of the third plane of Pt atoms.

Resonant coherent excitation was proposed by Okorokov [8] based on the simple notion that a periodic potential of a crystal channel or a crystal surface provides a frequency $\nu_r \propto v/d_{[hkl]}$ for an ion moving with a speed *v* along a chain of atoms with the lattice distance *d*. Equality is obtained by considering the possibility of different "harmonics" introducing a constant $k = 1, 2, 3, \ldots$, if the ion (or atom) has an excitation energy ΔE_{ij} where *i* and *j* represent the initial and final state the ion can be excited. The resonant energy E_r is then estimated from:

$$E_r[\mathrm{MeV}/\mu] = 3.03k^{-2}d^2[\mathrm{Å}^2]\Delta E_{ij}^2[\mathrm{keV}^2] \qquad (5)$$

For our case of $^{15}N^{6+}$ the excitation energy from 1s to 2*s*, 2*p* is 500 eV; the surface lattice constant of the $[1\bar{1}0]$ chains of Pt(110) is 2.772 Å, and hence E_r = 21.8 MeV for the second harmonic $k = 2$. Fig. 7 shows the "field" of resonances in the *E* versus ϕ plane where ϕ is the azimuthal angle of the ion beam with respect to the $[1\bar{1}0]$ surface direction. This field of resonances is calculated for a crystal with lattice constant a_0 from [27]:

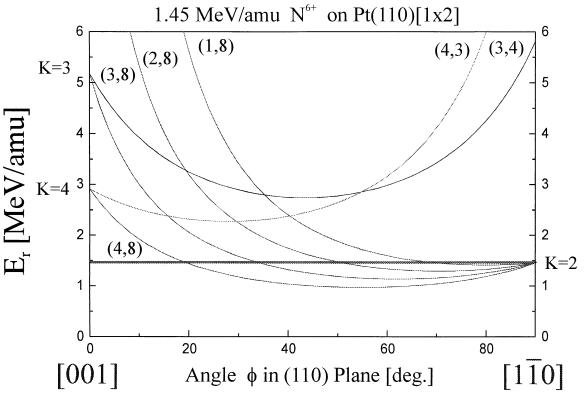

Fig. 7. Calculated resonance energies for 21.8 MeV N^{6+} scattering off Pt(110)(1 × 2) along different crystallographic orientations, i.e. for different azimuthal angles ϕ using Eq. (7). The numbers in brackets are the coefficients *l*, *m*. The horizontal line corresponds to the resonance condition of our experiment.

$$E_r[\mathrm{MeV}/\mu] = 3.03 a_0^2[\text{Å}^2]\Delta E_{ij}^2[\mathrm{keV}^2](l\cos\phi + m\sin\phi)^{-2} \quad (6)$$

where l and m are parameters taking the harmonics into account. For the reconstructed Pt(110)(1 × 2) surface Eq. 6 is modified, i.e.

$$E_r[\mathrm{MeV}/\mu] = 3.03 a_0^2[\text{Å}^2]\Delta E_{ij}^2[\mathrm{keV}^2](l/2\cos\phi + m\sqrt{2/4}\sin\phi)^{-2} \quad (7)$$

The excitation has for the case of the variation of the azimuthal angle a parallel and a transversal contribution. This leads to the appearance of "sidebands" [13,20].

An important consideration is the influence of the solid state electrons on ΔE_{ij}. It is known that the binding energies are shifted relative to the vacuum level by image forces and screening effects. Theoretical estimates show that the energies E_i and E_j are shifted indeed, but the ΔE_{ij} are hardly affected [28]. These theoretical results confirm the previous experimental findings, and ours for that matter, that Eq. 5 is a good approximation for an estimate of E_r. Another result of the theory concerns the coherence of the excitation. A certain length of the trajectories is required to reach the excitation. At other lengths the excitation may even be destroyed. For our case of $^{15}N^{6+}$ at 21.8 MeV, lengths of ≥100 nm are sufficient to reach about 15% excitation. In this context, also, the width of the resonances can be estimated [26] from the resonance function:

$$R_T = \sin[(\omega_{ij} - gv)T/2](\omega_{ij} - gv)^{-1} \quad (8)$$

where $g = 2\pi/a_0$ ($l\sin\phi + m\sin\phi$), $T \gg \omega_{ij}$ relates the required "resonance time" T with the energy of the atomic excitation in question. The results show that the resonance widths are sufficiently large to allow some deviations of experimental parameters like, e.g. the primary energy or the azimuthal angle ϕ from the exact values predicted by Eqs. (5) and (6).

4. Experimental results

With respect to the RCE effect we have two types of results. The first data we present are measured with the PSD. The PSD collects all scattered particles and a part of the primary beam. When the scattered particles and the part of the primary beam that is not blocked by the target pass through the magnetic sector field the different charge states are separated. If this is done for 23 MeV [Fig. 4(a) and (b)], the spatial patterns change position but nothing else happens, because at 23 MeV there is no capture or loss of electrons by the projectile. In the case of the 21.8 MeV beam we observe the splitting into three features on the PSD, i.e. part of the primary beam, N^{6+}, and N^{7+} ions (Fig. 8). For known magnetic fields the positions of the intensity maxima can be estimated. This allows positive identification of the charge state and the determination of the angle of incidence and the scattering angle. Depending on the azimuthal angle there is evidence for a variation of the N^{7+} yield with a maximum at the orientation $\phi = 0°$ which is the orientation along the closed packed rows of the Pt(110) surface. The counts in the N^{6+} and the N^{7+} spots are then summed up and the ratio $N^{7+}/(N^{6+} + N^{7+})$ is plotted versus ϕ (Fig. 9). Note that in this procedure there is no energy analysis of the scattered ions.

The energy analysis is provided by the SBD. The combination of the sector field magnet and the SBD is essentially a spectrometer. If the alignment of beam and target is achieved as in the case of the data obtained in Fig. 8, the PSD is removed and the SBD is moved into the beam. When varying the field strength, the part of the primary beam passing the target, the N^{6+} beam, and the N^{7+} beam are well separated (Fig. 5). The peaks of the scattering ions have a Gaussian shape, as expected from the fact that the ions are momentum analysed by the magnet. For probing the resonance using the SBD we set the magnet at the valley between the N^{7+} and N^{6+} peaks. This is the high energy part of the N^{7+} ions that should be the best channeled ions. These are ions that travel straight along the $\langle 1\bar{1}0\rangle$ chains. Other trajectory types involving zig-zag motions have higher energy

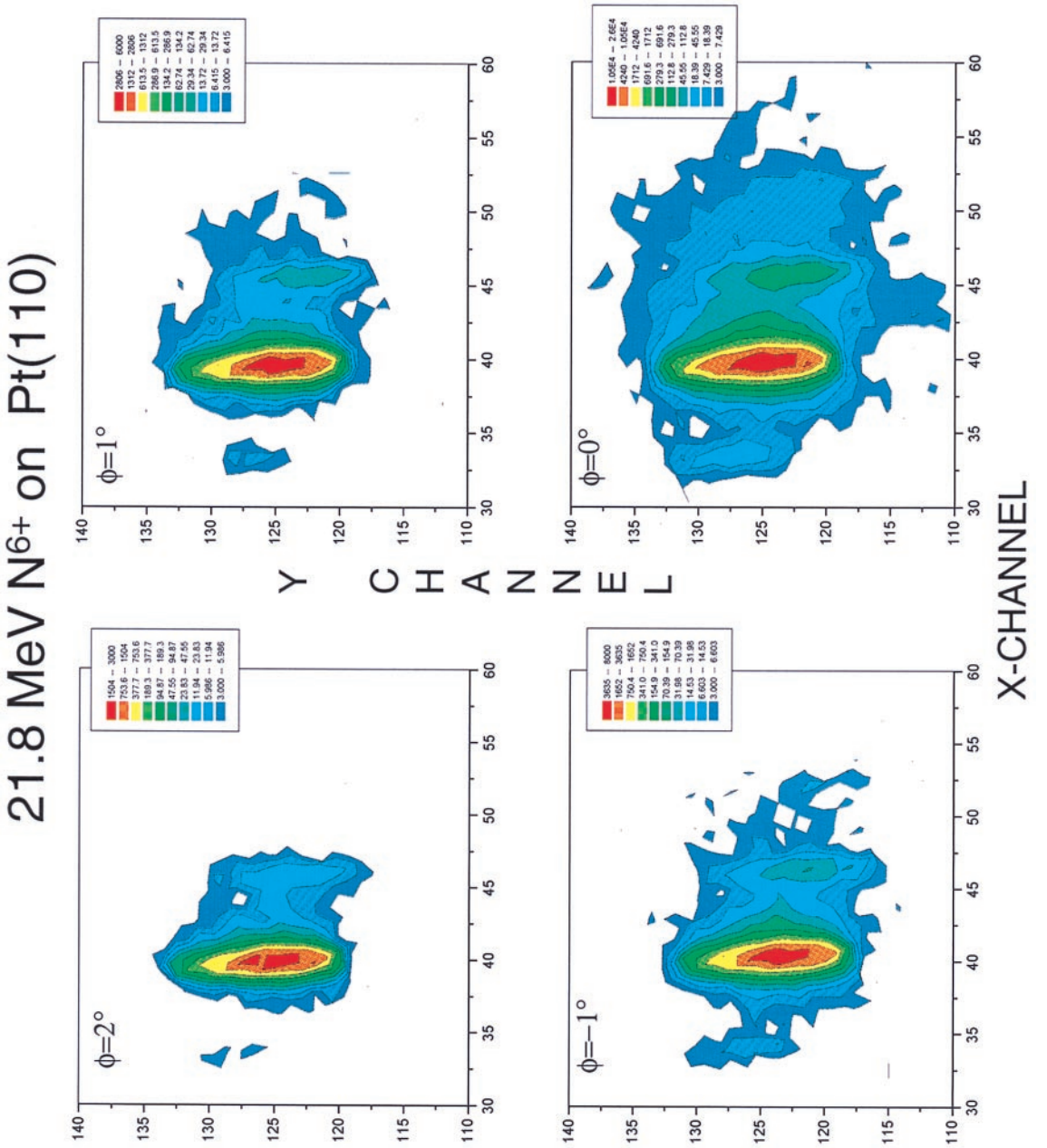

Fig. 8. Resonant coherent excitation (RCE) effect measured with the PSD for different azimuthal angles. The high intensity spot in the middle is approximately one half of the primary N^{6+} ions; the spots to the left are N^{7+} ions, the spots to the right are N^{6+} ions. Color code as in Fig. 4.

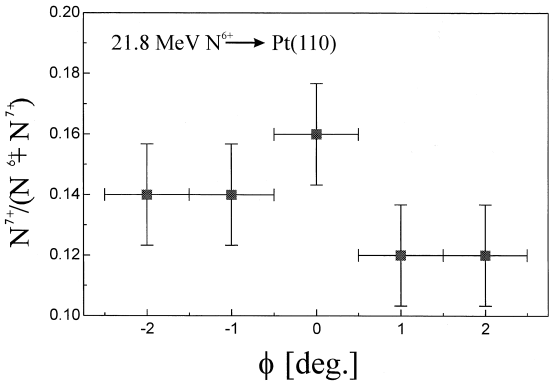

Fig. 9. The intensity ratio $N^{7+}/(N^{7+} + N^{6+})$ vs. ϕ around the $\langle 1\bar{1}0\rangle$ surface channels of Pt(110)(1 × 2) at $\phi = 0°$.

losses. For the N^{6+} ions we find in this part of the energy spectrum the ions with the highest energy loss. From our trajectory calculations we have evidence that these are the ions with the longest trajectories that include zig-zag trajectories. A spectrum taken at this specific setting of the magnetic field is shown in Fig. 10. The spectrum can be split into two Gaussian distributions with high accuracy. The accuracy gauged by the r^2 coefficient is $r^2 = 0.99$ for all spectra.

[Note: $r^2 = 1 - \Sigma_{i=1}^{n} (Y_i^{calc} - Y_i^{exp})^2/\Sigma_{i=1}^{n} (Y_i^{exp})^2$]. The results of the ion yield ratio $N^{7+}/(N^{7+} + N^{6+})$ for different angles of incidence ψ and for different azimuthal angles ϕ are summarized in

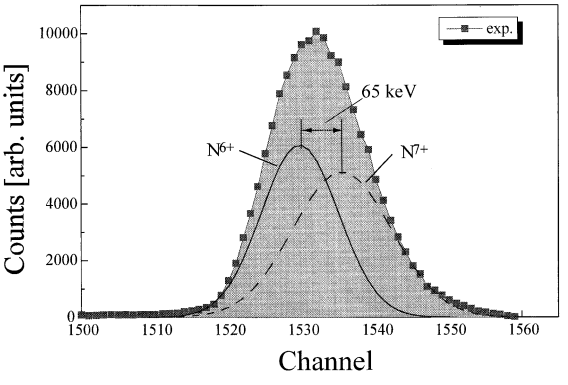

Fig. 10. SBD measured energy distribution at a magnetic field setting where energy distributions of the N^{6+} and of the N^{7+} ions overlap. The spectrum is fitted with two Gaussians.

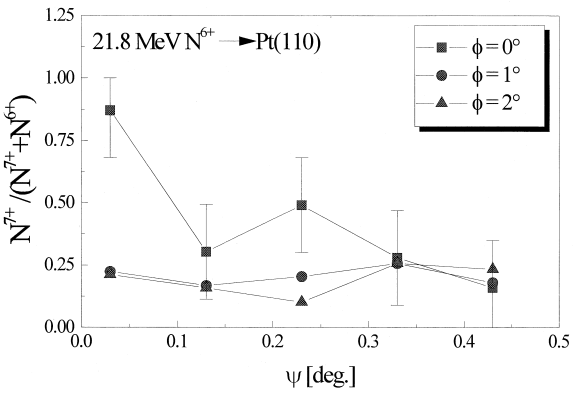

Fig. 11. The RCE effect from the SBD measurements as a function of the angle of incidence ψ and for three settings of the azimuthal angle ϕ ($\phi = 0°$) corresponding to the $\langle 1\bar{1}0\rangle$ surface channel direction.

Fig. 11. The RCE effect centers very sharply at $\phi = 0°$. The maximum is higher than in the case of the PSD results (Fig. 9) due to the trajectory selection via the magnet and the energy analysis by the SBD. With an increasing angle of incidence the resonance disappears due to the decrease of the trajectory lengths and the breakthrough that starts at approximately $\psi = 0.06°$ at 21.8 MeV.

5. Discussion

The data presented here have two aspects: (1) the surface channeling and (2) the RCE. With respect to (1) these are the highest energies for which surface channeling has been observed. For bulk channeling the highest energy reported is 33 TeV/c [29]. It is really worth considering how large an energy range can be understood by the same physical concept "invented" by Jens Lindhard [6]. The observation of channeling and the proof for it, is in our case coupled with the observation of RCE. Surface hyperchanneling is the condition sine qua non for the RCE to be observed.

The apparent intensity difference between the primary beam and the scattered beam [Fig. 4(b) or Fig. 8 at $\phi = 0°$] does not give the proper estimate of the channeled beam intensity. At an angle of incidence of

$\psi = 0.03°$ the crystal with a width of 10 mm presents a target with a height of 5×10^{-3} mm only. The maximal scattered beam intensity can hence be 2.5% of a beam of 0.2×0.2 mm^2. Experimentally (with the PSD) we find 1.55%, taking into account the fact that we cut half of the beam by the target setting. Compared to measurements in the keV range where we find 100% surface channeling [7,21] for $E_\perp = 10$ eV, about 60% of the particles are lost at 21.8 MeV. The disappearance of particles is due to steps on the target surface, as discussed previously [14,15]. Steps essentially present traps for channeled particles. Because the angles with respect to the surface are so small, channeled ions simply continue to channel at upward steps along their trajectories. The good news is that these ions will not come back out again because they are hyperchanneled. There is a chance, however, for ions passing through terraces of lengths that are short in comparison to typical ranges of N in Pt. These possible bulk channeling effects seem not to play a major role because there is no wide angle scattering visible on the PSD graphs, and there is also not much evidence for large energy losses in the SBD spectra. It is worth noting that on the PSD graphs the N^{7+} spots seem to be "smaller" than the N^{6+} spots, in agreement with the notion that the production of N^{7+} needs the best channeling. The evaluation of the SBD spectra is a future task because they contain information on the electronic energy loss processes at these rather high energies [30]. An interesting aspect in this respect is the fact that the N^{6+} ions do not change their charge during the scattering, i.e. we have the case of "frozen" charge state.

Acknowledgements

We thank N. Stolterfoht and G. Schiwietz (HMI), P. Sigmund (Odense), and S. Schippers (Gießen), for helpful discussions. Financial support was given by the Deutsche Forschungsgemeinschaft (DFG) and the EU.

References

[1] A. Arnau, F. Aumayr, P.M. Echenique, M. Grether, W. Heiland, J. Limburg, R. Morgenstern, P. Roncin, S. Schippers, R. Schuch, N. Stolterfoht, P. Varga, T.J.M. Zouros, HP. Winter, Surf. Sci. Rep. 27 (1997) 113.
[2] J. Burgdörfer, in Review of Fundamental Processes and Applications of Atoms and Ions, C. Lin (Ed.), World Scientific, Singapore, 1993, Chap. 11, p. 517.
[3] D. Niemann, M. Grether, A. Spieler, N. Stolterfoht, C. Lemell, F. Aumayr, HP. Winter, Phys. Rev. A 56 (1997) 4774.
[4] J. Limburg, Phys. Scr. T 73 (1997) 298.
[5] S.T. de Zwart, T. Fried, U. Jellen, A.L. Boers, A.G. Drentje, J. Phys. B 18 (1985) L623.
[6] J. Lindhard, K. Dansk, Vidensk. Selsk. Mat.-Fys. Medd. 34 (1965) 14.
[7] H. Niehus, W. Heiland, E. Taglauer, Surf. Sci. Rep. 17 (1993) 213.
[8] V.V. Okorokov, Pis'ma JETP II 4 (1965) 175.
[9] H.G. Berry, D.S. Gemmel, R.E. Holland, J.-C. Poizat, J. Remillieux, J.N. Worthington, Phys. Lett. A 49 (1974) 123.
[10] M. Mannami, H. Kudo, M. Matsushita, K. Ishii, Phys. Lett. A 64 (1977) 136.
[11] S. Datz, C.D. Moak, O.H. Crawford, H.F. Krause, P.F. Dittner, J. Gomez del Campo, J.A. Biggerstaff, P.D. Miller, P. Hvelplund, H. Knudsen, Phys. Rev. Lett. 40 (1978) 843.
[12] C.D. Moak, S. Datz, O.H. Crawford, H.F. Krause, P.F. Dittner, J.G. del Campo, J.A. Biggerstaff, P.D. Miller, P. Hvelplund, H. Knudsen, Phys. Rev. A 19 (1979) 977.
[13] S. Datz, P.F. Dittner, H.F. Krause, C.R. Vane, O.H. Crawford, J.S. Forster, G.S. Ball, W.G. Davies, J.S. Geiger, Nucl. Instr. Meth. B 100 (1995) 272.
[14] K. Kimura, H. Ida, M. Fritz, M. Mannami, Phys. Rev. Lett. 76 (1996) 3850.
[15] M. Mannami, K. Kimura, K. Narumi, M. Yamamoto, S. Naito, Nucl. Instrum. Methods B 125 (1997) 97.
[16] K. Kimura, S. Ooki, H. Ida, M. Mannami, Nucl. Instrum. Methods B 135 (1998) 413.
[17] Y. Martynenko, in Atomic Collision Phenomena in Solids, D.W. Palmer, M.W. Thompson, P.D. Townsend (Eds.), North Holland, Amsterdam, 1970, p. 400.
[18] N. Hatke, M. Dirska, M. Grether, E. Luderer, A. Robin, A. Närmann, W. Heiland, Phys. Rev. Lett. 79 (1997) 3395.
[19] N. Hatke, M. Dirska, E. Luderer, A. Robin, M. Grether, A. Närmann, W. Heiland, Nucl. Instrum. Methods B 135 (1998) 307.
[20] C. Auth, A. Mertens, H. Winter, A.G. Borisov, F.J. Garcia de Abajo, Phys. Rev. Lett. 79 (1998) 4477.
[21] A. Niehof, W. Heiland, Nucl. Instrum. Methods B 48 (1990) 306.
[22] N. Hatke, Thesis Universität Osnabrück, 1998.
[23] S. Speller, J. Kuntze, T. Rauch, J. Bömermann, M. Huck, M. Aschoff, W. Heiland, Surf. Sci. 366 (1996) 251.
[24] J.H. Barrett, Phys. Rev. B 3 (1971) 1527.
[25] M. Hou, M.T. Robinson, Appl. Phys. 17 (1978) 371.

[26] J.F. Ziegler, J.P. Biersack, U. Littmark, The Stopping and Range of Ions in Solids, Pergamon, New York, 1985, Vol. 1.
[27] E. Kupfer, H. Gabriel, J. Burgdörfer, Z. Phys. A 300 (1981) 35.
[28] F.J. Garcia de Abajo, Nucl. Instrum. Methods B 125 (1997) 1.
[29] G. Arduini, C. Biino, M. Clément, K. Cornelis, N. Coble, K. Elsener, G. Ferioli, G. Fidecaro, L. Gatignon, P. Grafström, M. Gyr, W. Herr, J. Klem, U. Mikkelsen, E. Weisse, S.P. Møller, E. Uggerhøj, A. Taratin, A. Freund, P. Keppler, J. Major, Phys. Rev. Lett. 79 (1997) 4182.
[30] N. Hatke, A. Robin, M. Grether, A. Närmann, W. Heiland, unpublished.